Mon. Not. R. Astron. Soc. **363,** 1398–1408 (2005) doi:10.1111/j.1365-2966.2005.09538.x

A submillimetre survey of Lyman α haloes in the SA 22 protocluster at $z = 3.1$

J. E. Geach,[1⋆] Y. Matsuda,[2] Ian Smail,[3] S. C. Chapman,[4] T. Yamada,[5] R. J. Ivison,[6] T. Hayashino,[7] K. Ohta,[2] Y. Shioya[8] and Y. Taniguchi[8]

[1]*Department of Physics, University of Durham, South Road, Durham DH1 3LE*
[2]*Department of Astronomy, Kyoto University, Sakyo-ku, Kyoto 606-8502, Japan*
[3]*Institute for Computational Cosmology, Durham University, South Road, Durham DH1 3LE*
[4]*Department of Physics, California Institute of Technology, MS 320-47, Pasadena, CA 91125, USA*
[5]*National Astronomical Observatory of Japan, Mitaka, Tokyo 181-8588, Japan*
[6]*Astronomy Technology Centre, Royal Observatory, Blackford Hill, Edinburgh EH9 3H5*
[7]*Research Center for Neutrino Science, Graduate School of Science, Tohoku University, Aramaki, Aoba, Sendai 980-8578, Japan*
[8]*Astronomical Institute, Graduate School of Science, Tohoku University, Aramaki, Aoba, Sendai 980-8578, Japan*

Accepted 2005 August 17. Received 2005 August 17; in original form 2005 April 21

ABSTRACT

We present the results from a submillimetre (submm) survey of a sample of 23 giant Lyman α (Lyα) emitting nebulae in the overdensity at $z = 3.09$ in the SA 22 field. These objects, which have become known as Lyα Blobs (LABs), have a diverse range of morphology and surface brightness, but the nature of their power source remains unclear, with both cooling flows or starburst/active galactic nucleus (AGN) ionized winds being possibilities. Using the Submillimetre Common-User Bolometer Array (SCUBA) submm camera on the James Clerk Maxwell Telescope (JCMT), we measure the 850-μm flux of a sample of LABs. We present detections of submm emission from four LABs at $>3.5\sigma$ individually, and obtain a modest statistical detection of the full sample at an average flux of 3.0 ± 0.9 mJy. These detections indicate significant activity within the LAB haloes, with bolometric luminosities in the ultraluminous regime ($>10^{12}\,L_{\odot}$), equivalent to a star formation rate (SFR) of $\sim 10^3\,M_{\odot}\,yr^{-1}$. By comparisons to LAB-like objects in other regions, we show that there is an apparent trend (although weak) between observed Lyα emission and bolometric luminosity. Combined with our detection of ultraluminous activity in this population and the lack of any strong morphological correlations in our sample, this provides evidence that the interaction of an ambient halo of gas with a Galactic-scale 'superwind' is most likely to be responsible for the extended Lyα emission in the majority of LABs. Assuming the extent of the LABs reflects outflows from a superwind, we estimate the age of starbursts in the submm LABs to be in the range 10–100 Myr. Using the average submm flux of the LABs, we determine an SFR density in the SA 22 structure of $>3\,M_{\odot}\,yr^{-1}\,Mpc^{-3}$, greater than the field at this epoch. The submm detection of these four LABs means there are now seven luminous submm galaxies in the $z = 3.09$ structure in SA 22, making this the largest known association of these intensely active galaxies. This clustering further strengthens the proposed evolutionary link between these galaxies and local cluster ellipticals. Finally, we suggest that the highly extended Lyα haloes (which define the LAB class) may be a common feature of the submm galaxy population in general, underlining their role as potentially important sources of metal enrichment and heating of the intergalactic medium (IGM).

Key words: galaxies: evolution – galaxies: haloes – galaxies: high-redshift – galaxies: starburst – cosmology: observations.

1 INTRODUCTION

Since the earliest X-ray spectroscopic observations of clusters of galaxies, it has been apparent that the intracluster medium (ICM)

⋆E-mail: j.e.geach@durham.ac.uk

in these systems contains a significant mass of metals. This material must have been processed through stars (most likely residing in galaxies) and then either expelled or removed from the stellar system. The apparent lack of evolution in the ICM metallicity in the high-density cores of clusters out to $z \sim 1$ (Mushotzky & Scharf 1997; Tozzi et al. 2003) points to an early phase of ICM enrichment for the highest density regions, while claims of a minimum entropy in the ICM (Ponman, Helsdon & Finoguenov 1999) support mechanisms which can transfer both energy and metals to the environment. Outflows or winds driven by star formation or active galactic nucleus (AGN) activity have been proposed as an efficient mechanism for dispersing metals from within galaxies and heating the surrounding gas. Local starburst galaxies such as M82 or Arp 220 are known to exhibit spatially extended structures, visible as haloes of emission-line gas and hot X-ray emitting gas. These are believed to be related to wind-driven outflows emerging from the active regions of these galaxies (Heckman, Armus & Miley 1990). If high-redshift galaxies are expelling considerable quantities of enriched material into their environments then similar emission-line structures may be visible around them.

Sensitive narrow-band surveys have uncovered a class of giant Lyman α (Lyα) emission-line nebulae at high redshift [Steidel et al. 2000 (S00); Matsuda et al. 2004 (M04)]. Both these surveys focus on an overdense structure at $z = 3.09$ discovered by S00 in the SA 22 field. This structure has been interpreted as a cluster in the process of formation (S00), and is therefore an excellent natural laboratory to study galaxy evolution. The extended and morphologically diverse features of the Lyα haloes in SA 22 have led them to be termed Lyα Blobs (LABs, S00). With luminosities of up to 10^{44} erg s^{-1} and physical extents of up to 100 kpc (S00), these objects have many of the properties expected for high-redshift analogues of the outflowing haloes seen in local galaxies – although their luminosities and sizes would need to be scaled up by at least an order of magnitude to match the high-redshift LABs.

Similarly, extended and luminous Lyα haloes have been found around bright radio galaxies at comparable redshifts using similar narrow-band imaging techniques (e.g. De Breuck et al. 1999; Kurk et al. 2000; Reuland et al. 2003). These haloes are interpreted as tracers of cooling and feedback in merging galaxies at high redshifts (Reuland et al. 2003), with their morphological diversity suggesting the active growth through mergers of these powerful radio galaxies. There is also strong evidence that many of these radio galaxies reside in high-density regions, as traced by overdensities of extremely red objects, Lyα emitters (LAEs), X-ray sources or submillimetre (submm) galaxies (e.g. Kurk et al. 2000; Smail et al. 2003; Stevens et al. 2003). Hence, there is some circumstantial evidence of a connection between large Lyα haloes and the earliest formation phase of the most massive galaxies in high-density regions at high redshifts.

M04 present a new catalogue of 35 LAB candidates over a 0.5 field at $z = 3.09$ in the SA 22 field from a narrow-band imaging programme using Suprime-Cam on the 8.2-m Subaru Telescope. This survey shows that LABs come in a range of sizes ($\sim$20–200 arcsec^2, $\sim$1150–11500 kpc^2) and have Lyα luminosities of the order 10^{42}–10^{44} erg s^{-1}. Their morphologies are complex, including filamentary structures, apparent bubbles and shells. Some LABs also appear to have associated continuum sources which may be capable of providing sufficient ultraviolet (UV) photons to power the emission-line halo, but some do not. Clearly, several possible mechanisms could produce a LAB, not just a wind, and several explanations of the physical processes governing the Lyα emission have been proposed: (i) photoionization by massive stars or an obscured AGN; (ii) cooling radiation from a collapsing gaseous halo (Fardal et al. 2001) or (iii) starburst superwind shock heating (Taniguchi & Shioya 2000; Ohyama et al. 2003). Additionally, it has been suggested that inverse-Compton scattering of cosmic microwave background photons by a population of relativistic electrons could also contribute (Scharf et al. 2004).

While each of these scenarios is potentially viable, one third of LABs are not associated with UV continuum sources, luminous enough to produce Lyα emission from photoionization (assuming a Salpeter initial mass function, M04), suggesting that the photoionization source in (i) would additionally need to be heavily obscured for these LABs, indicative of dust in the system. This is intriguing, since dust heavily suppresses Lyα emission, requiring that the Lyα emission originates well away from the obscuration, or that there is some other mechanism allowing Lyα photons to escape through the dust and into the observer's line of sight. The nature of the processes responsible for producing the extended Lyα emission in LABs thus remains uncertain.

The first LAB to be studied in detail was LAB1 in the SA 22 field [S00; Chapman et al. 2001 (C01); Chapman et al. 2004 (C04)]. LAB1 is the most luminous LAB catalogued in the SA 22 structure with a Lyα luminosity of $L_{\mathrm{Ly}\alpha} = 1.1 \times 10^{44}$ erg s^{-1} and also has the largest extent of all LABs identified to date, at $\sim$100 kpc. LAB1's morphology is complex, and it includes companion galaxies and other structures visible at high resolution in *Hubble Space Telescope (HST)* imagery from C04. There is now a wealth of multi-wavelength data available for this object. In particular, C01 show that there is a strong submm source coincident with the nebula ($S_{850} = 16.8 \pm 2.9$ mJy), confirming the presence of an extremely luminous power source within LAB1 with a bolometric luminosity in excess of 10^{13} L$_\odot$. C04 note that deep *Chandra* X-ray observations in the region of LAB1 failed to detect an X-ray counterpart – suggesting that the bolometric emission is not powered by an unobscured or partially obscured luminous AGN. However, they suggest that a heavily obscured AGN with a torus orientated at 45° to the sky might be responsible for the Lyα halo and would also explain extended linear features revealed by *HST* imaging, suggestive of jet-induced star formation.

Bower et al. (2004) used the SAURON integral field unit (IFU) to map the two-dimensional dynamics of the Lyα emission in LAB1, including the haloes of two associated Lyman Break Galaxies (LBGs, C11 and C15). These authors conclude that the nebula has a complex velocity structure which cannot be explained by a simple shell-like outflow; and that the submm source occupies a cavity in the Lyα halo, suggesting that either the region in the immediate vicinity of the submm galaxy (SMG) is obscured by dust ejecta, or it has completely ionized the material in this region.

The local surface density of 283 LAEs (smoothed with a Gaussian with a kernal of $\sigma = 1.5$ arcmin) at LAB1 is 0.63 arcmin^{-2} compared to the average density over the whole Suprime-Cam field of view of 0.39 arcmin^{-2} (Hayashino et al. 2004, M04). At a shallower limit, the density of the SA 22 Suprime-Cam field is 1.75 times that of the other blank (Subaru/*XMM–Newton* Deep Survey) field in Hayashino et al. (2004). Thus, the local density at LAB1 is 2.8 times that of the blank field. Since LAB1 is located at a peak in the underlying surface density, perhaps it is not surprising that this object is the brightest and largest of all known LABs – as it could represent a massive galaxy in the process of formation. It is equally possible that the large extent and complicated velocity structure of LAB1 is actually generated from several overlapping haloes related to C11, C15 and the submm source, which happen to inhabit the same dense region in the $z = 3.09$ structure.

The other LAB identified by S00 in the SA 22 structure is LAB2, it has a comparable Lyα luminosity to LAB1 and it has recently been shown to contain a hard X-ray source (Basu-Zych & Scharf 2004). These authors suggest that if the X-ray source is point-like, then the unabsorbed X-ray luminosity of $L_{\rm X} \sim 10^{44}\,{\rm erg\,s^{-1}}$ indicates that LAB2 harbours a supermassive black hole with a high local absorbing column. C01 also report submm emission from the vicinity of LAB2, but with a significantly lower submm flux than LAB1: $S_{850} = 3.3 \pm 1.2$ mJy (C01; C04). The detection of submm emission from both of the LABs studied to date may suggest a strong link between these two populations. This would clearly favour those models for the formation of LABs, which rely upon a highly active source to generate the extended emission-line halo. Perhaps more interestingly, if some LABs do not contain bolometrically luminous sources, then we must consider a variety of processes (cooling, photoionization, etc.) to account for these giant haloes. We have therefore undertaken a survey to detect or place limits on the submm emission from LABs at $z = 3.09$ in the SA 22 field.

The paper is organized as follows: Section 2 describes the LAB sample and data reduction, Section 3 contains our analysis, in Section 4 we discuss the results and in Section 5 we report our conclusions. Unless otherwise stated, we adopt a flat Universe with $\Omega_{\rm m} = 0.3$, $\Omega_\Lambda = 0.7$ and $H_0 = 70\,h$ km s^{-1} Mpc^{-1}, with $h = 1$. In this cosmology, the angular scale at $z = 3.09$ is 7.6 kpc arcsec^{-1} and the look-back time is 11.4 Gyr.

2 OBSERVATIONS AND DATA REDUCTION

Our selection was based on Subaru Suprime-Cam narrow-band imaging of a 34 × 27-arcmin^2 region around SA 22, which detected 33 new LABs (M04), in addition to the two LABs previously catalogued by S00. M04 obtained deep narrow- and broad-band imaging of this region using a narrow-band filter, NB497, and *B*-, *V*- and *R*-band filters with Suprime-Cam. The central wavelength of NB497 is 4977 Å, with a full width at half-maximum (FWHM) of 77 Å, sensitive to LAE over a redshift range of $z = 3.06$–3.13. By combining the *B*- and *V*-bands they were able to estimate the continuum emission in the narrow-band filter. This allows the construction of a continuum-subtracted, emission-line image by subtracting the *BV* image from the NB497 image. In this paper, we adopt the nomenclature of M04, who catalogue the 35 LABs in the order of descending isophotal area. In this system, LAB1 and 2 correspond to the 'blob 1' and 'blob 2' of earlier works (e.g. S00; C01).

We selected 13 of these LABs as targets for our submm observations. These were chosen to cover the full range of properties spanned by the LAB population (area, brightness, morphology and environment, see Table 1 and Fig. 1). To these 13 we have identified a further SMG, SMM J221735.84+001558.9, a submm source catalogued by Barger, Cowie & Sanders (1999), which corresponds to a Lyα-emitting microJansky radio source at $z = 3.09$ from Chapman et al. (2005). This SMG is coincident with the extended Lyα halo, LAB14, from M04. We note that Chapman et al. (2005) have detected a further SMG at $z = 3.098$ within the overdensity, SMM J221735.15+001537.2, with $S_{850} = 6.3 \pm 1.3$ mJy although this SMG has detectable Lyα emission, this is not sufficiently spatially extended to class as a LAB based on the selection of M04.

We used the National Radio Astronomy Observatory's[1] (NRAO) Very Large Array (VLA) to target SA 22 during 1998 October and 2003 July–September, obtaining 48 h of data at 1.4 GHz. The observations were taken for approximately 12 h in *B*-configuration and the remainder in *A*-configuration. The pseudo-continuum correlator mode '4' was employed, with 28 × 3.25-MHz channels, enabling us to map almost the entire primary beam (27.3 × 27.3 arcmin^2), recording data every 5 s in both left-circular and right-circular polarizations. 0137+331 was used to set the flux scale, with 2212+018 (2.8 Jy) used for local phase/amplitude/bandpass calibration.

Finally, in addition to our new submm photometry observations, we also take advantage of an existing shallow submm map to place limits on further nine LABs. In total, including the previously published studies of LAB1 and 2, we have submm observations of 25 LABs.

2.1 Submm observations

Observations were conducted using the Submillimetre Common User Bolometer Array (SCUBA) on the James Clerk Maxwell Telescope (JCMT) over the nights of 2004 September 18–22. SCUBA was used in photometry mode to search for 850- and 450-μm emission from the 13 LABs listed in Table 1. We employed two-bolometer chopping, whereby the on- and off-source positions are divided between three bolometers to maximize the signal-to-noise (S/N) ratio in the final coadded flux measurement (discussed further in Section 2.2). Our goal was a mean rms noise in our measurements of ∼1.5 mJy – requiring ∼2–3 ks integration in Grade 1–2 weather conditions ($\tau_{\rm CSO} \leqslant 0.08$, $\tau_{850} \leqslant 0.32$).

To achieve sky and background cancellation we chopped in azimuth by 60 arcsec. Calibration observations employed Uranus and zenith opacity was measured from regular skydips and the JCMT water vapour monitor, yielding $\tau_{850} \leqslant 0.25$ for all observations, with $\tau_{850} \sim 0.1$ for some portions of the run. The on-sky exposure times were 2.2 ks for all sources, which in the conditions we experienced yielded mean 1σ noise limits of 1.5 and 13 mJy at 850 and 450 μm, respectively.

We also obtained S_{850} fluxes or limits for 10 additional LABs (LAB8, 9, 11, 16, 19, 25, 26, 31 and 35; see Table 1) which were not observed in photometry mode, but do fall within a shallow, submm scan-map of SA 22 (Chapman & Borys, private communication). The map data were taken in a combination of SCUBA jiggle map and raster map modes at 850 μm during a number of observing runs with good observing conditions ($\tau_{850} < 0.09$). Some of the SCUBA jiggle maps are described in detail in Barger et al. (1999) and Chapman et al. (2001, 2003, 2004). The combination of these SCUBA jiggle and raster maps is described in Chapman et al. (2003), using the approach of Borys et al. (2003). This map covers an 11 × 11-arcmin^2 region approximately centred on LAB1 and has a conservative rms depth of ∼5.3 mJy at 850 μm – it therefore is only sensitive enough to detect the brightest submm sources, such as that residing in LAB1. We extract the fluxes from the calibrated map by measuring 15-arcsec diameter aperture fluxes and converting these using an assumed Gaussian beam profile to give fluxes in Jy beam^{-1}. In Fig. 1, we plot the sky distribution of all 35 LABs from M04, indentifying those which are map or photometry observations.

2.2 Data reduction

Standard routines from the SCUBA User Reduction Facility (SURF, Jenness & Lightfoot 1998) were used to reduce each LAB photometry observation. For both long and short arrays (850 and 450 μm), demodulated data were flat-fielded and corrected for atmospheric

[1] NRAO is operated by Associated Universities, Inc., under a cooperative agreement with the National Science Foundation.

Table 1. The catalogue of LABs in the SA 22 region observed in the submm. We give the coordinates, 850-μm fluxes, isophotal Lyα emission areas and Lyα luminosities for LABs in the full sample. LABs detected at $>3.5\sigma$ significance at 850 μm are shown in bold-face type. For comparison, we also note the results for the well-studied LAB1 and 2. We also classify the objects based on a simple morphological/Lyα luminosity description: F/C (faint+compact), F/E (faint+extended), B/C (bright+compact) and B/E (bright+extended), see Section 3.1. The compact–extended boundary is 50 arcsec^2 (2900 kpc^2), and the faint–bright boundary is 10^{43} erg s^{-1}. Note: 10^{44} erg s^{-1} $= 2.6 \times 10^{10}$ L$_\odot$.

Name	RA (J2000) (h m s)	Dec. (J2000) (d ′ ″)	S_{850} (mJy)	Area[a] (arcsec^2)	log $_{10}$ $L^b_{\rm Ly\alpha}$ (erg s^{-1})	log $_{10}$ $L^c_{\rm bol}$ (erg s^{-1})	Luminosity/ morphology	Notes[d]
LAB1	**22 17 24.68**	**+00 12 42.0**	**16.8 ± 2.9**	**222**	**44.04**	**47.06**	**B/E**	**2 companion LBGs**
LAB2	22 17 39.00	+00 13 27.5	3.3 ± 1.2	152	43.93	<46.39	B/E	Hard X-ray source
LAB3	22 17 59.15	+00 15 29.1	−0.2 ± 1.5	78	43.76	<46.48	B/E	Lyα emitter (LAE)[e]
LAB4	22 17 25.12	+00 22 11.2	0.9 ± 1.5	57	43.58	<46.49	B/E	
LAB5	**22 17 11.67**	**+00 16 44.9**	**5.2±1.4**	**55**	**43.23**	**46.55**	**B/E**	**LAE**
LAB6	22 16 51.42	+00 25 03.6	−0.5 ± 1.8	42	43.20	<46.56	B/C	LAE
LAB7	22 17 40.99	+00 11 26.9	0.2 ± 1.6	40	43.18	<46.51	B/C	
LAB8	22 17 26.18	+00 12 53.5	0.3 ± 5.3	39	43.23		B/C	MAP
LAB9	22 17 51.09	+00 17 26.2	1.3 ± 5.3	38	43.11		B/C	LAE, MAP
LAB10	**22 18 02.27**	**+00 25 56.9**	**6.1±1.4**	**34**	**43.34**	**46.61**	**B/C**	**LAE**
LAB11	22 17 20.33	+00 17 32.1	−0.4 ± 5.3	30	42.96		F/C	MAP
LAB12	22 17 31.90	+00 16 58.0	3.2 ± 1.6	29	42.93	<46.52	F/C	
LAB14	**22 17 35.91**	**+00 15 58.9**	**4.9± 1.3**	**27**	**43.08**	**46.52**	**B/C**	**LAE, C05**
LAB16	22 17 24.84	+00 11 16.7	2.2 ± 5.3	25	43.00		B/C	LAE, MAP
LAB18	**22 17 28.90**	**+00 07 51.0**	**11.0 ± 1.5**	**22**	**42.81**	**46.87**	**F/C**	Possible X-ray source
LAB19	22 17 19.58	+00 18 46.5	−8.6 ± 5.3	21	43.11		B/C	LAE, MAP
LAB20	22 17 35.30	+00 12 49.0	0.4 ± 1.5	21	42.81	<46.49	F/C	
LAB25	22 17 22.59	+00 15 50.8	1.4 ± 5.3	19	42.77		F/C	MAP
LAB26	22 17 50.43	+00 17 33.4	−2.7 ± 5.3	18	42.79		F/C	MAP
LAB27	22 17 06.96	+00 21 31.1	0.5 ± 1.6	18	42.83	<46.50	F/C	
LAB30	22 17 32.44	+00 11 34.1	3.3 ± 1.3	17	42.98	<46.41	F/C	
LAB31	22 17 38.94	+00 11 02.0	−3.7 ± 5.3	17	43.04		B/C	LAE, MAP
LAB32	22 17 23.88	+00 21 56.5	1.8 ± 1.4	17	42.76	<46.46	F/C	LAE
LAB33	22 18 12.56	+00 14 33.3	1.6 ± 1.5	16	42.95	<46.49	F/C	
LAB35	22 17 24.84	+00 17 17.0	1.2 ± 5.3	16	42.95		F/C	LAE, MAP

[a]M04 – isophotal area determined on corrected narrow-band emission-line map. [b]M04 – luminosity at $z = 3.09$. [c]Bolometric luminosity determined from S_{850}, assuming a modified blackbody with $T_{\rm d} = 40$ K, $\alpha = 4.5$ and $\beta = 1.7$.[d]Taken from the literature: S00, M04, Hayashino et al. (2004) and Chapman et al. (2005). MAP = SCUBA scan-map extracted flux, see Section 3.1. [e]Associated optical LAE from Hayashino et al. (2004).

extinction. A sky-estimate was subtracted using REMSKY by subtracting the average (median) signal from all the off-source bolometers in the arrays (avoiding any dead or noisy bolometers). Subtracting the sky-estimate gave a marginally better S/N ratio than not removing it. Finally, a 6σ clip was applied to remove spikes before the signals were coadded. For calibration, we derived the flux conversion factor (FCF) from the observations of Uranus using the FLUXES program.

The chopping technique we adopted splits the on-source integration over two bolometers in an attempt to maximize the exposure time spent on the source. After the FCF was applied, an inverse-variance weighting scheme was applied to combine the two signals. Compared to the S/N ratio from the main signal bolometer, on an average the S/N ratio improved after combining by ∼14 per cent for S_{850} and ∼8 per cent for S_{450}. We list the fluxes measured for the LABs in Table 1. Note that the flux densities in Table 1 do not include uncertainties due to absolute flux calibration, which we estimate to be ∼10 per cent.

For the VLA data, editing and calibration were performed using standard AIPS procedures. We then employed IMAGR to map the central region, together with 40 satellite fields, running several iterations of the self-calibration procedure described by Ivison et al. (2002). Finally, we corrected for the primary beam response using PBCOR. The final image has a series of north–south stripes, as described by C04, but this affects none of the LABs discussed here. The typical noise level is around 9 μJy beam^{-1}, where the beam has an FWHM of 1.4 arcsec.

At the $\gtrsim 4\sigma$ level, the only detections amongst our sample are of LAB1 (as described by C04) and LAB4, which have several weak radio sources near the position listed in Table 1, as well as a stronger source to the south-east. The remainder of the LAB sample discussed here have upper limits at 1.4 GHz of around $5\sigma < 45$ μJy (for unresolved sources).

3 ANALYSIS AND RESULTS

3.1 Submm emission

In Table 1, we summarize the results of our submm observations, along with other information collected from the literature. In addition to the photometry mode observations, we tabulate the fluxes extracted from the SCUBA scan-map, and the previously published 850-μm fluxes of LAB1 and 2 from Chapman et al. (2000). We detect three LABs from the photometry-mode targets with S_{850} fluxes detected at significances of $>3.5\sigma$: LAB5, 10 and 18. A further target, LAB30, has a flux corresponding to 2.6σ, but we do not classify this as a formal detection. No individual LABs are detected at 450 μm and therefore we have not tabulated individual 450-μm results.

To these three new detections, we can also add a fourth submm-detected LAB, LAB14. This source was detected in jiggle-map observations by Barger et al. (1999) with an 850-μm flux of 4.9 ± 1.3 mJy (Chapman et al. 2005). The SMG was included in

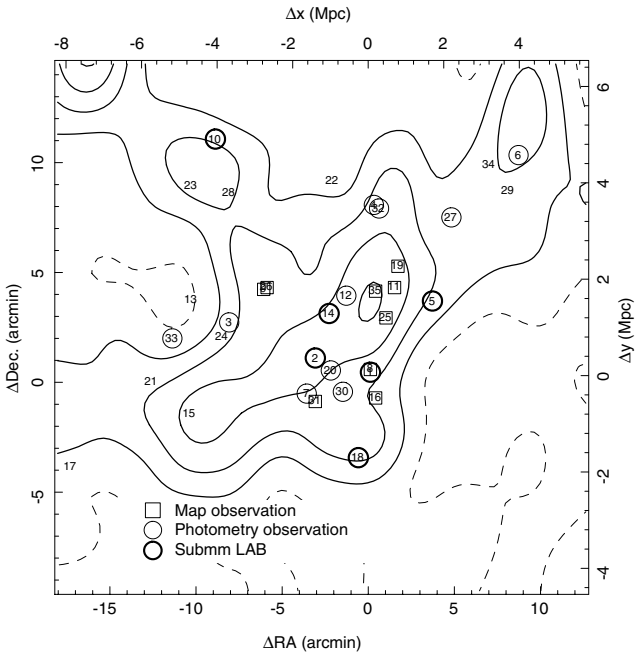

Figure 1. The sky distribution of the 35 known LABs in SA 22 from M04. Photometry observations are circled, map observations are identified with squares and submm-detected LABs are circled in bold (Section 3.1). The contours represent the surface density of the underlying LAE distribution: solid (dashed) contours show regions of greater (less) than average surface density in steps of 50 per cent of the average surface density. We discuss the environments of LABs further in Section 3.4. The origin of the coordinates is centred on LAB1, and the physical scale corresponds to angular separation.

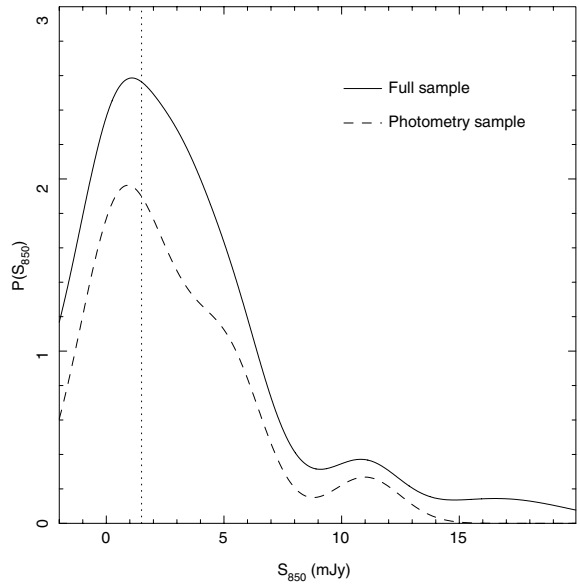

Figure 2. The S_{850} flux distribution of LABs in the sample. Here we have represented the distribution in terms of a superposition of Gaussian probability distributions for the full sample (solid line) and just the photometry sample (dashed line). The photometry sample only includes those objects targeted with SCUBA in 'photometry' mode, whereas the full sample includes LAB1 and 2 and the map extractions. The vertical dotted line indicates the 1σ 850-μm noise limit for the photometry sample.

the redshift survey of submm galaxies by Chapman et al. (2003, 2005). They identified the counterpart as a Lyα-emitting galaxy at $z = 3.089$, and cross-correlation of their position with the LAB catalogue of M04 shows that this SMG has an extended Lyα halo. We can thus add four submm-detected LABs to the two previously known.

Looking at the distribution of 850-μm fluxes for the entire sample, Fig. 2, we note that there is an excess of positive flux measurements for our sample. We confirm this by deriving a noise-weighted average 850-μm flux for the LABs observed in photometry mode of 2.8 ± 0.9 mJy, where the uncertainty is derived by bootstrap resampling. A more rigorous test is provided by removing the well-detected LABs, averaging the fluxes of the remainder gives a mean flux of 1.2 ± 0.4 mJy. Similarly, when LAB1, 2 and 14 and the fluxes of those sources covered by the scan-map are included in this analysis the average flux is 3.0 ± 0.9 mJy (we note that our bootstrap errors are conservative compared to the noise-weighted rms values). Thus, we have $\geqslant 3\sigma$ detections of the LAB samples with typical fluxes around the level of the blank-field SCUBA confusion limit.

Performing a similar analysis on the 450-μm fluxes for the photometry sample yields a noise-weighted average of 6.2 ± 2.1 mJy, giving a 3σ detection of the whole sample at 450 μm. The noise-weighted mean 450/850-μm flux ratio is $S_{450}/S_{850} = 3.1 \pm 2.8$. This is consistent with a dust temperature of $T_{\rm d} \sim 40$ K at $z = 3.09$ (assuming a dust emissivity index of 1.5).

We can convert the average 850-μm flux of the LABs into a typical luminosity using the characteristic dust temperature of $T_{\rm d} \sim 40$ K derived above and knowing that the LABs are at $z = 3.09$. We estimate the typical LAB (with a Lyα luminosity of 6×10^{42} erg s^{-1} or $1.6 \times 10^9\,{\rm L}_\odot$) has a bolometric luminosity of $5.4 \times 10^{12}\,{\rm L}_\odot$. If this emission arises wholly from star formation with a standard IMF (Kennicutt 1998), then this luminosity corresponds to a star formation rate (SFR) of $\sim$900 $\rm M_\odot\,yr^{-1}$.

We note that the lack of radio detections for the majority of LABs is consistent with these estimates. Empirically scaling the spectral energy distributions (SEDs) of either Arp 220 or M82 to our average 850-μm flux for a source at $z = 3.1$ implies 1.4-GHz fluxes of 15–35 μJy – below our detection limit.

3.2 Individually detected LABs

Here we discuss the properties of the individual LABs from our sample. We show the Lyα emission-line images (from M04) of a selection of the LABs in our photometry sample in Fig. 3. Note that the SCUBA beam size is 15 arcsec.

3.2.1 LAB5

LAB5 is a large halo, the second largest submm-detected LAB after LAB1, but much fainter and more diffuse than LAB1. There is some evidence for a slight elongation of the Lyα emission (Fig. 3), but the halo overall is roughly circular and the brightest region corresponds to a faint continuum source in the centre of the halo. LAB5 is located near the peak in the surface density of LAEs (Fig. 1).

3.2.2 LAB10

LAB10 has a relatively compact morphology, and is within about 5 arcsec of an extended, bright continuum source. It is unclear whether these objects are related, but if they are independent, then the submm detection of LAB10 combined with the lack of an extended diffuse halo offers several possibilities for its power source: (i) LAB10 is in the initial stages of luminous activity (i.e. the start

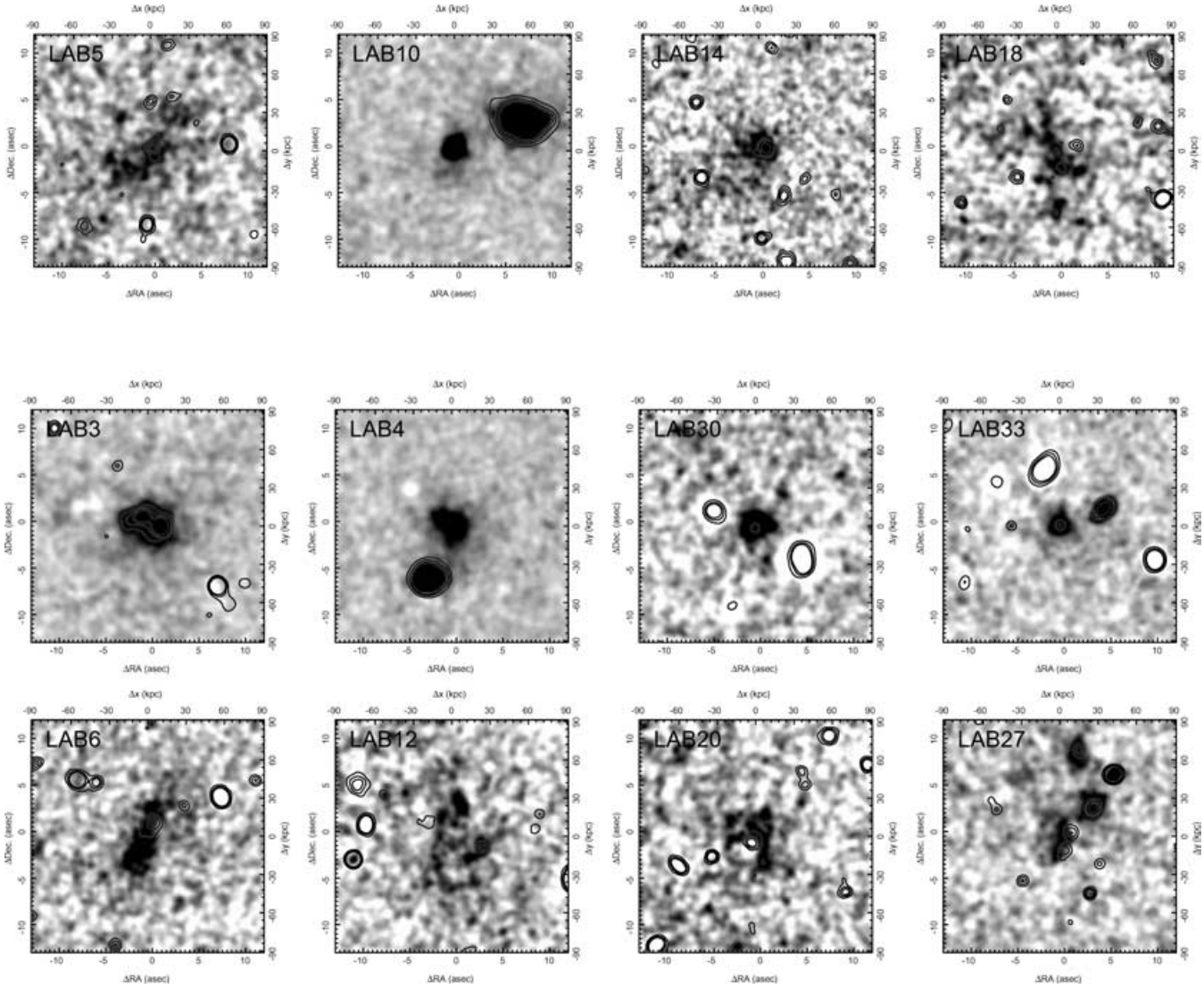

Figure 3. Narrow-band Lyα imaging of a subset of the LABs in our submm photometry sample with submm emission (top row) and without detected submm emission (bottom two rows). In this figure, we divide the non-detected LABs into two morphological categories: in the top row we show LABs which are compact, with undisturbed haloes; and in the bottom row we show LABs with more complex morphologies – these objects exhibit more elongated and complex structure than the compact objects. Grey-scale denotes the Lyα line emission corrected for continuum emission, first presented in M04 (see Section 2 for a description), while the contours show the location of continuum emission at levels of $\sim$3, 5 and 7σ. The intensity scales are identical, each panel is 25×25 arcsec^2($\sim$190 $\times$ 190 kpc) and have north at the top and east to the left. The panels are centred on the coordinates listed in Table 1.

of a starburst or AGN), and is expelling a wind which has so far only progressed a small distance into the intergalactic medium (IGM); (ii) the fact that LAB10 is compact is an orientation effect: we are looking face-on to a jet or collimated wind emerging from the SMG. A cooling flow cannot be ruled out, but the fact that this LAB has a significant 850-μm flux (corresponding to an SFR of $\sim$1600 $M_\odot$ yr^{-1}) is a strong circumstantial evidence that the Lyα halo is related to the obscured activity in this source.

Whereas the majority of LABs reside close to the main peak in the underlying distribution of LAEs (see Fig. 1), LAB10 lies in a secondary peak which resembles a filamentary structure to the north-west, connected to the main bulk of the protocluster.

3.2.3 LAB14

The submm source in LAB14 was identified from cross-correlating the LAB catalogue in M04 with the redshift survey of SMGs (Chapman et al. 2005). Its morphology is compact, and comprises a bright component with a diffuse $\sim$50-kpc long extension to the south-east. The source has a bolometric luminosity of 8.7 $\times$ 10^{12} $L_\odot$, making this an ultraluminous-class active galaxy. As with LAB5, LAB14 is located close to the peak of the surface density of LAEs.

3.2.4 LAB18

This is the strongest submm source in the photometry sample (S_{850} = 11.0 $\pm$ 1.5 mJy) and has an apparently hourglass Lyα morphology. It is the second brightest LAB, after LAB1, in terms of its submm emission. It does not possess a continuum counterpart, which suggests that either its ionizing source is completely dust-enshrouded, or that the power for the Lyα emission is from a superwind. Unlike LAB1, this object does not have companion LBGs, which may contribute to the large measured extent of LAB1. LAB18's Lyα

luminosity is lower than LAB1. We note from Fig. 1 that LAB18 appears to reside in a much lower density environment (reflected in the projected surface density of LAEs) compared to the other LABs.

Using archival *XMM–Newton* data (PI: O. Almaini) of the SA 22 field, we tentatively detect a hard X-ray source at the location of LAB18 with a (0.4–10 keV) flux of $\sim 6 \times 10^{-15}$ erg cm $^{-2}$ s^{-1} at the $\sim 2\sigma$ level. The measured flux is consistent with the X-ray flux of LAB2 (Basu-Zych & Scharf 2004) and corresponds to $L_{\rm X} \sim 5 \times 10^{44}$ erg s^{-1} if we assume a photon index of 1.5 and local absorbing column $n_{\rm H} = 4.8 \times 10^{20}$ cm^{-2} as did those authors. We do not detect X-ray emission from any other LABs in this sample. If this detection is confirmed then it would suggest that LAB18 harbours a luminous, obscured AGN which may contribute to the submm emission and which could also couple with the ambient gas in the galaxy's halo.

3.2.5 *Non-detected SMGs*

Although our study hints at submm emission from LAB12 and 30 at the $\sim$2–2.5σ level, the majority of the LABs we targeted with our photometry observations were not detected. These non-detections could be down to the uncertainty in where the submm source lies within the LAB – this is a particular concern for the largest and most irregular LABs – although the large size of the SCUBA beam and the flux aperture we adopted means we are relatively insensitive to offsets of less than $\sim$5 arcsec; or insufficient sensitivity in our submm observations. The fact that we obtain a 3σ detection of the stacked submm emission from the stacked sources at a flux level of $\sim$3 mJy suggests that insufficient depth is likely to be a contributing cause to the non-detection of all but the brightest LABs.

3.3 Lyα properties of LABs

We now search for the correlations in the submm detection rate and the properties of LABs as a function of their Lyα properties to identify trends which might indicate the nature and origin of their extended haloes. Therefore, in Table 2 we compare the properties of detected ($>3.5\sigma$) and undetected LABs. We do this both for those LABs in our photometry sample and also for the full sample including LAB1, 2 and 14 and the limits from the submm map.

The first point to note from Table 2 is that there appears to be no difference in the isophotal area of the Lyα emission (measured from the continuum-corrected narrow-band images) or Lyα luminosities between LABs with detected submm emission and those without. Including LAB1 does affect the area significantly, but since this object is the largest known, it could be considered a 'special' object and not typical of LABs in general.

We can also perform the reverse test, to determine the submm emission from different samples of LABs differentiated by the extent and brightness of their Lyα haloes. We therefore provide a simple classification based on their isophotal areas and Lyα luminosities. First, we assign four categories: bright-compact (B/C), bright-extended (B/E), faint-compact (F/C) and faint-extended (F/E). The bright–faint boundary is 10^{43} erg s^{-1} and the extended–compact boundary is 50 arcsec^2 (2800 kpc^2). The noise-weighted average 850-μm flux for each category is presented in Table 3. Again, we perform this analysis for just the photometry observations, and the full sample including LAB1, 2 and 14 and map observations. There are no F/E LABs in this scheme, in part due to the fact that F/E LABs fall below the sensitivity limit of M04's narrow-band survey. There appears to be no difference between any of these area/luminosity classes.

Table 2. The mean properties of LABs detected and undetected at $S_{850} > 3.5\sigma$. We give the values for the LABs from our photometry observations, and in '[]' we include data from LAB1, 2 and 14 and the extracted fluxes from the map. The S_{850} values are noise-weighted averages and all errors are bootstrapped.

	$\log_{10} \langle L_{\rm Ly\alpha} \rangle$ (erg s^{-1})	$\langle$Area$\rangle$ (arcsec^2)	$\langle S_{850} \rangle$ (mJy)
Detected	43.13 ± 0.14	37 ± 8	7.3 ± 1.5
	$[43.30 \pm 0.16]$	$[72 \pm 31]$	$[7.1 \pm 1.4]$
Un-detected	43.10 ± 0.09	34 ± 7	1.2 ± 0.4
	$[43.09 \pm 0.08]$	$[36 \pm 7]$	$[1.4 \pm 0.4]$

Table 3. 850-μm fluxes (in mJy) of LABs based on a simple morphological luminosity classification: the bright–faint boundary is 10^{43} erg s^{-1} and the extended–compact boundary is 50 arcsec^2 (2900 kpc^2). We give values for the LABs from our photometry observations, and in '[]' values which include LAB1, 2 and 14 and our extracted map fluxes. The mean fluxes listed here are noise weighted and the errors are estimated from bootstrap resampling.

	Bright	Faint
Extended	2.2 ± 1.4	...
	$[3.3 \pm 1.4]$	[...]
Compact	2.4 ± 1.8	3.2 ± 1.3
	$[2.8 \pm 1.5]$	$[3.0 \pm 1.2]$

To look at this question in more detail, we also study the morphologies of the Lyα haloes for the detected and non-detected submm sources (Fig. 3). Generally, the morphologies of the LABs fall into two classes – those with an elongated or apparently disturbed halo (e.g. LAB5, 12 and 18), and those which are compact and less disturbed (e.g. LAB3, 10 and 30). The submm-detected LABs have a range of morphology: LAB5 and 18 are elongated and diffuse, whereas LAB10 and 14 are more compact and circular. To show that the morphologies are not a significant factor for the submm emission, we note that each of the four submm-detected LABs has a morphological counterpart in the non-detected sample (e.g. LAB5 versus LAB6 or LAB10 versus LAB4).

In summary, we can find no property of the Lyα emission from the LABs, which correlates strongly with their submm detection rate or flux. However, given our statistical detection of submm emission in the whole sample, implying starburst/AGN activity in a large proportion of LABs, it seems likely that this bolometrically luminous activity must have some relationship with the LAB haloes. For example, if a wind is responsible for the emission, then we may be observing various stages of LAB evolution, governed by the nature and environment of the submm source.

3.4 Environmental properties of LABs

To determine any trend in the environments of the submm-detected LABs, we compare them to the local surface density of 283 LAEs at $z = 3.09$ in SA 22 from M04 in Fig. 1. The contours compare the local density of LAEs to the average density over the field of view. The LAE distribution was convolved with a Gaussian with a comoving size of $\sigma = 2.8$ Mpc. The bold contours indicate regions of greater than average local surface density, clearly showing the filamentary large-scale structure in the protocluster.

Although LAB1 resides close to a node in the large-scale structure (Matsuda et al., in preparation), we find no tendency for the

other submm-detected LABs to reside in higher density local environments than the average LAE, suggesting that this behaviour is not reflected in the wider sample. Indeed, if anything it might be argued that our new submm-detected LABs lie in lower density regions on an average, although this is not statistically significant. We note that although the underlying density field may not be correlated with the positions of LABs, the local density may have an effect on the properties of LABs, which may account for the range of sizes and luminosities we observe.

4 DISCUSSION

We now discuss the wider insights which our observations provide into the properties and origin of LABs and their environments. We concentrate on the interaction of winds generated from luminous activity within the embedded SMGs with the ICM as the most likely source of Lyα emission.

4.1 LAB formation mechanisms

In Fig. 4, we plot the Lyα luminosity against the bolometric luminosity calculated for the submm-detected LABs – LAB1, 5, 10 and 14. We have also plotted the flux of the submm-undetected LABs from our stacking analysis and two objects which are proposed to be similar to LABs: the SCUBA galaxy N2-850.4 (Keel et al. 1999; Smail et al. 2003a) and the *Spitzer*-identified source SST24 J1434110+331733 (Dey et al. 2005). We discuss these analogous

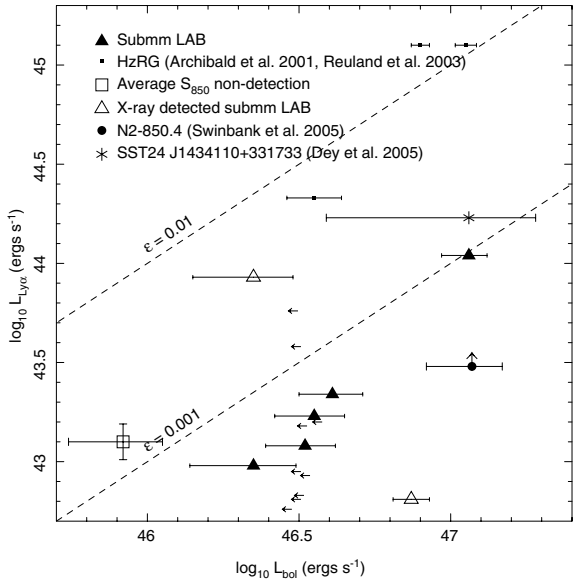

Figure 4. Lyα luminosity versus bolometric luminosity (assuming a modified blackbody with $T_{\rm d} = 40$ K, $\alpha = 4.5$ *and* $\beta = 1.7$) for submm-detected LABs and potentially related objects. Note that we plot LAB30 as a submm-detected LAB, and 3σ upper limits are plotted for the remainder of the photometry sample. Also shown is the flux obtained from stacking the submm-undetected LABs from the photometry sample. The starburst galaxy N2-850.4 (Smail et al. 2003a; Swinbank et al. 2005) is also shown, along with the *Spitzer* detected source SST24 J1434110+331733: both these objects have been identified with extended Lyα haloes. The dashed lines show a simple model where the Lyα luminosity is determined as a fraction ϵ of the bolometric luminosity. We show this model for the scenarios $\epsilon = 0.01$ and 0.001. We also plot three submm-detected, high-redshift radio galaxies with extended Lyα emission for comparison.

systems further in Section 4.4.[2] The bolometric luminosities of the LABs are calculated by integrating over a modified blackbody curve with a dust temperature of 40 K and $(\alpha, \beta) = (4.5, 1.7)$.

This analysis allows us to examine any causal connection between the bolometric output of the LAB and the luminosity of the Lyα halo. As Fig. 4 shows there is a weak trend between $L_{\rm bol}$ and the luminosity of the extended Lyα haloes for the sample – in the sense that the most bolometrically luminous sources have more luminous associated Lyα haloes.

We adopt a simple model in which the Lyα emission traces a fraction ϵ of the bolometric luminosity, where ϵ combines the fraction of energy output by star formation or AGN which generates a wind and the fraction of that wind energy which produces Lyα emission: $L_{\rm Ly\alpha} = \epsilon L_{\rm bol}$. In Fig. 4, we plot this behaviour for values of ϵ corresponding to 1 and 0.1 per cent of the bolometric output. A fractional output around $\sim$0.1 per cent best describes the LABs, indicating that only a small proportion of the bolometric output from the obscured activity in these galaxies is required to support these luminous haloes. The weak trend we see is consistent with a direct causal link between the extended Lyα emission and that from the obscured sources detected in the submm. The most likely mechanism which could provide this link is winds (Ohyama et al. 2003) and we suggest that winds are the major cause of the extended Lyα emission seen in the LAB population. This proposal would indicate that LABs may be found around a large range of the submm population and we explore this idea further in Section 4.4.

Clearly the trend shown in Fig. 4 is not a tight correlation. There are several possible explanations for this – including different efficiencies for coupling energy to the halo from different sources (e.g. AGN or starbursts), potentially cyclic activity, environmental influences and observational uncertainties. We provide a more quantitative discussion on the mechanics of emergent winds and jets, and possible environmental influences on the luminosity of Lyα haloes in the next section. We note that the two LABs with possible X-ray counterparts – LAB2 and 18 – are not well described by the general trend. These are the two LABs whose tentative X-ray detections suggest that they may contain obscured AGN (upper limits for the remainder of the population are consistent with the measured fluxes and luminosities of these two marginal detections). This might explain why they depart from the trend in Fig. 4 (i.e. AGN may interact differently with the ICM than starbursts). However, the fact that they lie respectively above and below the trend suggests that other factors may be at work, in particular, their local environments. Fig. 1 shows that LAB18 lies in one of the lowest density regions in our survey, while LAB2 is close to the peak in the LAE distribution. LAB18 has a submm flux $\sim$3 times that of LAB2, but the Lyα luminosity of LAB2 is over an order of magnitude greater than LAB18. This suggests that although a powerful embedded submm source might be required for the generation of a LAB, it may be the local environment (i.e. the density of ambient intracluster gas) which governs the efficiency of coupling of the bolometric output to the luminosity of the halo. This is a natural explanation for the apparent diversity of the properties of these objects. Unfortunately, our survey is

[2] We note that the extremely red object 2142-4420 B1 (Francis et al. 2001) also has been identified with an extended halo ($L_{\rm Ly\alpha} \sim 10^{44}$ erg s^{-1}). Those authors suggest that the far-infrared (FIR) emission of the embedded galaxy could be of the order 5×10^{47} erg s^{-1}, although a precise FIR luminosity is not available. If this predicted FIR luminosity is correct then it would place the source at a similar location to SST24 in Fig. 4.

too sparse to conclusively test for environmental influences on the properties of submm-bright LABs.

To demonstrate the potential variation in $L_{\mathrm{Ly}\alpha} - L_{\mathrm{bol}}$, which may arise from AGN-driven activity, we also plot on Fig. 4 three high-redshift radio galaxies (HzRGs) from Reuland et al. (2003) with detected 850-μm emission from Archibald et al. (2001), converted to our cosmology. These galaxies show a much higher ratio of Lyα emission at a fixed bolometric output, compared to the LABs indicating the role of powerful radio jets and possible contributions from inverse-Compton ionization (Scharf et al. 2004) in addition to the starburst or AGN activity, shown by the LABs.

4.2 Origin of the wind

In this paper, we have used the term 'wind' to refer to the interaction between any outflowing material whatever its origin and the IGM (or the young, ICM in the case of SA 22). Are there any observational signatures to distinguish the feedback of starbursts and AGN on the ICM? AGNs are very localized – they can impart energy into the galaxy via direct irradiation or jets: highly collimated outflows from matter accretion on to a black hole. Starbursts are more complex, in the sense that the energy release can be distributed over a wider volume (in giant molecular clouds), and comprises the output of young massive stars, and a contribution from an enhanced supernovae (SNe) rate. For an AGN, on larger scales the most likely mechanism for generating an outflow is expected to be jets breaking out of the galaxy and into the IGM. These outflows entrain material from the galaxy (in the case of SMGs this would include dust) and the IGM, and create a shock front when they become supersonic in the ambient medium. It is this shock which can heat the ambient gas to ionizing temperatures, and therefore dissipates the jet's energy. In this situation the observations will be orientation specific, such that a face-on jet-induced LAB will be compact and bright, whereas a side-on jet might resemble an elongated structure. The morphological diversity of the LABs could be explained by this variety of mechanisms, with both these observational classes being found in our sample (e.g. LAB10 and 18, respectively), although it is unclear whether an AGN, starburst, or combination of the two is responsible. We note that without detailed spectroscopic evidence to unravel the kinematics of these systems, caution must be exercised in our wind analysis: similar structures could be easily explained by the distribution of tidal material resulting from a merger.

Starburst-driven winds can emerge from a galaxy and interact with the IGM in a similar way to an AGN jet. Although not as concentrated, these winds can still be collimated, and resemble jets with a very wide opening angle (at least for local FIR luminous galaxies, e.g. Heckman et al. 1990). For these collimated winds, a similar orientation dependence governs observations, but the loose collimation allows the formation of the extended diffuse haloes present in several of these LABs (e.g. LAB5 and 6). The escape of Galactic winds from dusty, high-redshift starburst galaxies might be different to their lower redshift counterparts (e.g. M82), and we must take that into account when considering these scenarios. Given that it is possible for AGN and starbursts to generate similar morphological structures in LABs and so with our present observational tools we cannot clearly distinguish between AGN- and starburst-powered winds in the LABs. However, if the obscured activity seen in the LAB population is exactly analogous to that in typical submm galaxies at this epoch, then from detailed studies of the AGN in the latter population we can conclude that it is likely that star formation is responsible for the winds in the LABs (Alexander et al. 2005; Swinbank et al. 2005).

4.3 Energy injection, mass loss and age

Heckman et al. (1990) discuss the mechanics of emergent superwinds from the discs of a sample of low-z FIR galaxies. Those authors present a simple model for the energy injection rate (into some ambient medium) from the inflation of a bubble due to the combined effect of stellar winds from massive stars and the detonation of SNe: $\mathrm{d}E/\mathrm{d}t \sim 3 \times 10^{41}\, r^2 v^3 n_0\ \mathrm{erg\ s^{-1}}$, where r is the radius of the bubble in kpc, v is the wind velocity in units of $100\,\mathrm{km\,s^{-1}}$ and n_0 is the density of the undisturbed medium just outside the bubble in $\mathrm{cm^{-3}}$. Applying this to our sample; if we take the radius of the bubble in LABs to be the extent of the emission (in this case between ∼10–100 kpc with a median of 22 kpc), a wind velocity of $\sim$1000 km s^{-1} (characteristic of the escape velocity from a massive galaxy) and a density of 1 cm^{-3} (Shull & McKee 1979), then the energy injection rate is of the order 10^{45} erg s^{-1}. The typical luminosities of LABs in this sample are approximately two orders of magnitude lower than this, suggesting that the conversion of bolometric energy to Lyα emission (via winds) is an inefficient process. The conversion efficiency from bolometric to Lyα luminosity derived from the trend in Fig. 4 is ∼0.1 per cent, which would support this interpretation. We note that the effect of the density of the ambient medium on the injection rate is vital in this analysis – a lower ambient density favours a lower coupling of bolometric luminosity (that is generated by the starburst or AGN) and a wind into the IGM. This would provide a natural explanation of the fact that there is significant scatter in the trend between L_{bol} and $L_{\mathrm{Ly}\alpha}$. For example LAB18, which resides in a much lower density environment compared to the rest of the LABs, has a high bolometric luminosity (second only to LAB1), but a much lower Lyα luminosity.

This simple wind model allows us to estimate the age of the starburst (or AGN activity) by comparing the extent of the haloes with the velocity of the superwind. For the figures estimated above, these LABs could have starbursts of the age ∼20 Myr – although could be up to ∼100 Myr for the largest LABs. Caution must be exercised for this interpretation due to the fact that a halo might remain as an emission-line nebula for some time after luminous activity has ceased, or when cyclic models of activity are considered, a succession of which may have illuminated a halo at some former time, but which is now fading. None the less, starbursts of this age are consistent with estimates for other SMGs (e.g. >10 Myr for N2-850.4, Smail et al. 2003).

4.4 LABs around the submm population in general

About 20 per cent of the LABs in our (photometry) sample contain strong submm sources. Combined with the apparent trend between Lyα and FIR emission, and the morphological analysis, this supports the interpretation that a Galactic superwind is responsible for the Lyα emission. We speculate that giant Lyα emission-line haloes may be a feature of the general submm population.

Spectroscopic observations of SCUBA galaxies based on radio identification (Chapman et al. 2005) have yielded impressive results, with the redshifts of ∼100 galaxies currently known. An interesting feature of the spectra is the presence of strong Lyα emission lines, which aids in the measurement of redshifts. For example, in Chapman et al's spectroscopic survey of SMGs, of the 73 successful identifications, 34 per cent of them were made primarily with the Lyα line. This runs counter to the expectation that the active regions in submm galaxies should be heavily obscured by dust resulting from an intense starburst, and hence these regions are unlikely to be strong Lyα sources since dust efficiently destroys Lyα photons. The

presence of the Lyα line then suggests two possibilities: (i) the dust coverage is patchy, and Lyα photons generated within the galaxy escape through holes in the distribution (Chapman et al. 2004); or (ii) the Lyα emission originates well away from the dust in a halo coupled to the galaxy. This latter scenario is consistent with the LAB picture and would suggest that extended Lyα haloes should be found around many SMGs.

There already exists some evidence for extended Lyα haloes around luminous, FIR galaxies at high redshifts: the first submm-selected galaxy, SMM J02399-0136 (Ivison et al. 1998), also has a large Lyα halo, covering virtually all of the 15-arcsec slit used by those authors. Similarly, Smail et al. (2003b) detect four SMGs within $\sim$1 Mpc of the radio galaxy 53W002 ($z = 2.39$), and identify one of them, SMM J17142+5016, as a narrow-line AGN with an extended Lyα halo. Finally, the SCUBA galaxy N2-850.4 (SMMJ163650.43+405734.5, Ivison et al. 2002; Scott et al. 2002; Smail et al. 2003a) is a hyperluminous-class infrared (IR) galaxy undergoing a starburst at $z = 2.385$. There appears to be a diffuse Hα (and perhaps Lyα) halo surrounding the galaxy, which although apparently compact, may extend to large distances with a surface brightness below the limit of the observations. For comparison, we plot N2-850.4 in Fig. 4, using a lower limit for the Lyα luminosity of $>3 \times 10^{43}$ erg s^{-1} (Swinbank et al. 2005), and $L_{\rm bol} \simeq L_{\rm FIR} = 3.1 \times 10^{13}\,{\rm L}_{\odot}$ (Chapman et al. 2005).

Very recently, Dey et al. (2005) identified a *Spitzer Space Telescope* source, SST24 J1434110+331733, which is surrounded by a 200-kpc diameter Lyα nebula at $z \sim 2.7$. The nebula has $L_{\rm Ly\alpha} \sim 1.7 \times 10^{44}$ erg s^{-1} and the nebula hosts a bright mid-infrared source ($S_{24\,\mu{\rm m}} = 0.86$ mJy), with an implied FIR luminosity of $L_{\rm FIR} \sim 1 - 5 \times 10^{13}\,{\rm L}_{\odot}$, although the estimate is uncertain as it involves an order-of-magnitude extrapolation. The size and luminosity of the Lyα halo, combined with the potentially hyperluminous source lying within it make this a close analogue of LAB1. We plot it for comparison in Fig. 4, and note that it follows the trend shown by the majority of submm-detected LABs. This close association between a luminous, obscured source and a highly extended Lyα halo further supports our proposal that LABs may be a common feature of the high-redshift FIR population.

For completeness, however, we should note that our survey of SA 22 contains at least one submm source which does not appear to be associated with an extended halo. SMMJ221735.15+001537.2 is detected with $S_{850} = 6.3 \pm 1.3$ mJy (Chapman et al. 2005) at $z = 3.098$. Lyα is detected for this system, but it is not sufficiently extended to qualify as a LAB. The lack of spatial extent would be consistent with the picture where this is a young submm source and the wind has only just started to propagate into the IGM, thus resulting in a small or faint halo. Alternatively, as discussed above, local environmental conditions could play a role in the lack of emission we observe.

4.5 Star formation in the SA 22 region

Our detection of submm emission from the average LAB in our survey within the SA 22 field also allows us to compare the SFR density within this structure to that of the field at this epoch. To estimate the volume containing the $z = 3.09$ structure in SA 22, we assume that the star formation is contained within a comoving sphere of apparent size 15 arcmin, corresponding to a volume of $\sim 1.1 \times 10^4$ Mpc^3.

Directly integrating the submm emission from the six detected LABs (1, 2, 5, 10, 14 and 18) and the other SMG known to lie at $z = 3.09$ in this field (Chapman et al. 2005), we derive a total SFR in submm galaxies of $\sim 1.4 \times 10^4\,{\rm M}_{\odot}\,{\rm yr}^{-1}$. This yields an SFR density in SA 22: $\rho_{\rm SFR} > 1.3\,{\rm M}_{\odot}\,{\rm yr}^{-1}\,{\rm Mpc}^{-3}$. Alternatively, given our average submm flux for LABs of $\sim$3.1 mJy, the entire M04 catalogue of LABs would yield an SFR density of $\rho_{\rm SFR} > 3.2\,{\rm M}_{\odot}\,{\rm yr}^{-1}\,{\rm Mpc}^{-3}$ [SFRs are calculated assuming $L_{\rm bol} \sim L_{\rm IR}$ after Kennicutt (1998)].

A lower limit to the average SFR density at $z \sim 3$ is provided by UV-selected surveys of LBGs at this epoch, giving an SFR density of $\geqslant 0.1\,{\rm M}_{\odot}\,{\rm yr}^{-1}\,{\rm Mpc}^{-3}$ (Steidel et al. 1999) after accounting for dust extinction and extrapolating the LBG luminosity function to faint limits. Alternatively, we can use submm surveys to attempt to determine the SFR density from a bolometrically selected sample at this epoch, although at the cost of extrapolating the submm luminosity function. The spectroscopic survey of SMGs by Chapman et al. (2005) indicates an average SFR density at $z \sim 3$ of $\sim 0.8\,{\rm M}_{\odot}\,{\rm yr}^{-1}\,{\rm Mpc}^{-3}$. The estimates of the SFR density within the SA 22 structure indicate significant acceleration of early star formation in this overdense region (Ivison et al. 2000; Smail et al. 2003b; Stevens et al. 2003).

5 CONCLUSIONS

We have presented results from a submm SCUBA survey of a sample of 23 giant, Lyα emission-line nebulae – LABs – at $z = 3.09$ in the SA 22 protocluster. In addition to the previously studied LAB1 and 2 which have been shown to contain submm sources, we identify a published submm source with LAB14 and from our photometry observations we detect a further three (LAB5, 10 and 18) with 850-μm fluxes $>3.5\sigma$. We conclude the following.

(i) We have tripled the number of LABs with detected submm emission in the SA 22 overdensity to a total of six sources. The $z = 3.1$ protocluster in SA 22 is thus the richest association of submm galaxies known.

(ii) The majority of LABs contain sources which are undergoing an episode of extreme luminous activity; most likely caused by a starburst (although our current limits cannot rule out a contribution from an AGN) and are heavily obscured by dust.

(iii) The average 850-μm flux for the full sample of LABs is 3.0 ± 0.9 mJy, corresponding to SFRs of the order $10^3\,{\rm M}_{\odot}\,{\rm yr}^{-1}$. We also find a significant detection of submm emission from those LABs which are individually undetected in our submm observations.

(iv) We estimate that the SFR density in SA 22 is $\gtrsim 3\,{\rm M}_{\odot}\,{\rm yr}^{-1}\,{\rm Mpc}^{-3}$. This compares to recent estimates of $0.8\,{\rm M}_{\odot}\,{\rm yr}^{-1}\,{\rm Mpc}^{-3}$ for the obscured SFR at this epoch (Chapman et al. 2003, 2005), indicating an acceleration of star formation in the SA 22 structure at this early time.

(v) We find a trend between the Lyα luminosity of the haloes and the FIR luminosity of the embedded SMGs. This trend can be simply modelled in a scheme where a fraction ϵ of the bolometric output is converted to Lyα emission. For LABs, this fraction appears to be of the order $\sim$0.1 per cent. The existence of this trend suggests a causal link between the submm activity we detect and the extended Lyα haloes.

(vi) Galactic-scale 'superwinds' generated from the combined effect of stellar winds from massive stars and the detonation of SNe in the starburst, provide a natural explanation of the properties we see. These mechanisms would allow the IGM in the densest regions to be heated and enriched with metals at early times, in accordance with the observed lack of evolution in intracluster metallicity in the high-density cores of clusters out to $z \sim 1$ (e.g. Tozzi et al. 2003).

Finally, we examine the implications of the discovery of a large number of submm sources associated with LABs and propose that large emission-line haloes might be a common feature of the submm population in general (and perhaps all active galaxies in rich environments), implying strong feedback and outflows into the local environment from these galaxies. Lyα haloes such as these are then excellent candidates for further studies of feedback systems at high redshift, and an essential stage of galaxy evolution.

ACKNOWLEDGMENTS

The authors wish to thank Mark Swinbank, Richard Wilman, Richard Bower, Cedric Lacey and Masahiro Nagashima for helpful discussions, and Alastair Edge and Marek Gierlinski for help in analysing the *XMM–Newton* data. We thank an anonymous referee for useful comments which improved the clarity of this work. JEG is supported by a PPARC studentship. IRS acknowledges support from the Royal Society. This work made use of the Nasa Extragalactic Database (NED) which is operated by the Jet Propulsion Laboratory, Caltech, under contract with the National Aeronautics and Space Administration.

REFERENCES

Alexander D. M., Chartas G., Bauer F. E., Brandt W. N., Simpson C., Vignali C., 2005, MNRAS, 357, L16
Archibald E. N., Dunlop J. S., Hughes D. H., Rawlings S., Eales S. A., Ivison R. J., 2001, MNRAS, 323, 417
Barger A. J., Cowie L. L., Sanders D. B., 1999, ApJ, 518, L5
Basu-Zych A., Scharf C., 2004, ApJ, 615, L85
Borys C., Chapman S., Halpern M., Scott D., 2003, MNRAS, 344, 385
Bower R. G. et al., 2004, MNRAS, 351, 63
Chapman S. C. et al., 2000, MNRAS, 319, 318
Chapman S. C., Lewis G. F., Scott D., Richards E., Borys C., Steidel C. C., Adelberger K. L., Shapley A. E., 2001, ApJ, 548, L17
Chapman S. C. et al., 2003, ApJ, 585, 57
Chapman S. C., Scott D., Windhorst R. A., Frayer D. T., Borys C., Lewis G. F., Ivison R. J., 2004, ApJ, 606, 85
Chapman S. C., Blain A. W., Smail I., Ivison R. J., 2005, ApJ, 622, 772
De Breuck C., van Breugel W., Minniti D., Miley G., Rottgering H., Stanford S. A., Carilli C., 1999, A&A, 352, L51
Dey A. et al., 2005, ApJ, 629, 654
Dunlop J. S., Hughes D. H., Rawlings S., Eales S. A., Ward M. J., 1994, Nat, 370, 347
Fardal M. A., Katz N., Gardner J. P., Hernquist L., Weinberg D. H., Davé R., 2001, ApJ, 562, 605
Francis P. J. et al., 2001, ApJ, 554, 1001
Hayashino T. et al., 2004, AJ, 128, 2073
Heckman T. M., Armus L., Miley G. K., 1990, ApJS, 74, 833
Ivison R. J. et al., 1998, ApJ, 494, 211
Ivison R. J., Dunlop J. S., Smail I., Dey A., Liu M. C., Graham J. R., 2000, ApJ, 542, 27
Ivison R. J. et al., 2002, MNRAS, 337, 1
Jenness T., Lightfoot J. F., 1998, in Albrecht R., Hook R. N., Bushouse H. A., eds, ASP Conf. Ser. Vol. 145, Astronomical Data Analysis Software and Systems VII. Astron. Soc. Pac., San Francisco, p. 216
Keel W. C., Cohen S. H., Windhorst R. A., Waddington I., 1999, AJ, 118, 2547
Kennicutt R. C., 1998, ARA&A, 36, 189
Kurk J. D. et al., 2000 A&A, 358 L1
Leitherer C. et al., 1999, ApJS, 123, 3
Matsuda Y. et al., 2004, AJ, 128, 569
Mushotzky R. F., Scharf C. A., 1997, ApJ, 482, L13
Ohyama Y. et al., 2003, ApJ, 591, L9
Ponman T. J., Helsdon S. F., Finoguenov A., 1999, in Giuricin G., Mezzetti M., Salucci P., eds, ASP Conf. Ser. Vol. 176, Observational Cosmology: The Development of Galaxy Systems. Astron. Soc. Pac., San Francisco, p. 64
Reuland M. et al., 2003, ApJ, 592, 755
Scharf C. A., Smail I., Ivison R. J., Bower R. G., 2004, in Mulchaey J. S., Dressler A., Oemler A., eds, Carnegie Observatories Astrophys. Ser. Vol. 3, Clusters of Galaxies: Probes of Cosmological Structure and Galaxy Evolution. Carnegie Observatories, Pasadena, http://www.ociw.edu/ociw/symposia/series/symposium3/proceedings3.html
Scott S. E. et al., 2002, MNRAS, 331, 817
Shull J. M., McKee C. F., 1979, ApJ, 227, 131
Smail I., Chapman S. C., Ivison R. J., Blain A. W., Takata T., Heckman T. M., Dunlop J. S., Sekiguchi K., 2003a, MNRAS, 342, 1185
Smail I., Scharf C. A., Ivison R. J., Stevens J. A., Bower R. G., Dunlop J. S., 2003b, ApJ, 599, 86
Steidel C. C., Adelberger K. L., Giavalisco M., Dickinson M., Pettini M., 1999, ApJ, 519, 1
Steidel C. C., Adelberger K. L., Shapley A. E., Pettini M., Dickinson M., Giavalisco M., 2000, ApJ, 532, 170
Stevens J. A. et al., 2003, Nat, 425, 264
Swinbank A. M. et al., 2005, MNRAS, 284
Taniguchi Y., Shioya Y., 2000, ApJ, 532, L13
Tozzi P., Rosati P., Ettori S., Borgani S., Mainieri V., Norman C., 2003, ApJ, 593, 705

This paper has been typeset from a TEX/LATEX file prepared by the author.